

## ПОЛУЧЕНИЕ УЛУЧШЕННЫХ СЕЙСМИЧЕСКИХ ИЗОБРАЖЕНИЙ МЕТОДОМ ДИФРАКЦИОННОГО СУММИРОВАНИЯ ДЛЯ СЛОЖНОЙ СТРУКТУРЫ, СОДЕРЖАЩЕЙ ГРЯЗЕВОЙ ВУЛКАН, НА ЮГО-ВОСТОЧНОМ ПОБЕРЕЖЬЕ КАСПИЙСКОГО МОРЯ

Мердад Солеймани

*Professor assistant, Faculty of Mining, Petroleum and Geophysics,  
Shahrood University of Technology, Shahrood, Iran,*

Повышение качества и разрешающей способности сейсмических изображений сложнопостроенных геологических объектов представляет собой непростую задачу. Результаты идентификации границ соляных диапиров, разрывных нарушений, складчатых систем, покровных и шарьяжных зон, а также несогласного залегания толщ, как правило, неоднозначны и надежность их довольно низкая. Для решения этих проблем при построении сейсмических изображений применяются различные современные методы обработки: обращение полных волновых полей, восстановление волнового поля на основе интеграла Фейнмана, обратновременная миграция, оптимальное суммирование по общей отражающей площадке и т. д. Метод суммирования по общей отражающей площадке часто используется для характеристики сложных сред. Однако помимо преимуществ, позволяющих улучшить качество сейсмических изображений, этот метод сталкивается с проблемой падения наклонных границ в разные стороны. Оператор суммирования по общей отражающей площадке представляет собой приближенный сейсмический отклик криволинейной границы в неоднородной среде. В настоящей работе предлагается новый подход, который позволяет полностью решить проблему различных наклонов границ в сложнопостроенных сейсмических средах. В отличие от метода суммирования по общей отражающей площадке, новый оператор суммирования является приближением дифрагированного сигнала от точечного рассеивающего объекта на глубине. Для точки рассеивания определяются кинематические атрибуты волнового поля, но при этом не обеспечивается полный учет кривизны границы. В предлагаемом методе оператор суммирования вводится для каждого дифрагированного луча, направленного от точки рассеивания к поверхности. Таким образом, в новом операторе учитывается энергия, которая оказалась бы неучтенной при построении изображений с помощью других упрощенных операторов суммирования. Новый метод был использован для сейсмического моделирования сложной геологической структуры, включающей грязевой вулкан на юго-восточном побережье Каспийского моря. В районе встречается множество грязевых вулканов, которые указывают на наличие коллекторов природного газа. Глинистое вещество поглощает сейсмическую энергию, что снижает качество полученного глубинного разреза и делает проблематичным точное изображение объектов в области границы грязевых вулканов. Проблема была решена с помощью нового метода суммирования по общей рассеивающей площадке, в котором в разрезе учитывается вся энергия, включая энергию дифрагированных волн. Затем к суммированному разрезу применяется процедура миграции после суммирования по глубине. Полный глубинный разрез, полученный в результате этой процедуры, демонстрирует преимущества нового оператора суммирования для построения сейсмических изображений сложных объектов. В заключение можно сделать вывод, что предложенный метод применим для идентификации резких секущих отражающих границ, связанных с разрывными нарушениями, диапирами и участками несогласного залегания пород.

*Различные наклоны границ, общая отражающая площадка, общая рассеивающая площадка, сложнопостроенные среды, построение сейсмических изображений, Южно-Каспийская впадина.*

### SEISMIC IMAGE ENHANCEMENT OF MUD VOLCANO BEARING COMPLEX STRUCTURE BY THE CDS METHOD, A CASE STUDY IN SE OF THE CASPIAN SEA SHORELINE

Mehrdad Soleimani

Improving seismic image quality in complex geological structures remains a challenge in seismic imaging. In complex media, imaging of geological structures such as the boundary of salt diapirs, faults, folding systems, overthrust zones, and unconformities are controversial and challenging tasks. Therefore, new imaging methods such as full waveform inversion, path-integral seismic imaging, reverse time migration, and the optimized common reflection surface stack methods were introduced to face these challenges. The common reflection surface stack method was used frequently to resolve some of the problems in complex structure seismic imaging. However, besides its great advantage in enhancing the quality of seismic section, it faces a problem with conflicting dips. The common reflection surface stack operator is an approximation of the reflection response of a curved interface in an inhomogeneous medium. In this study, a new strategy in the common reflection surface

stack is introduced, which completely resolves the problem of conflicting dips in complex structures. Compared to the common reflection surface stack, the new stacking operator is the approximation of diffraction response of a diffraction point in depth. The kinematic wavefield attributes are defined for that diffraction point, whereas curvature of the interface is not fully considered. In the introduced strategy, there would be a stacking operator for each diffraction ray from the diffractor to the surface. Thus, the new operator gathers more energy that might get lost in imaging due to simplified operator in the other methods. The new method was applied to seismic data from a complex geological mud volcano bearing structure from south east of the Caspian Sea shoreline. This area includes numerous mud volcanoes which act as indicators of gas reservoirs. As a natural phenomenon, mud absorbs the seismic energy and deteriorates the quality of the final seismic section. Therefore, obtaining accurate image of the subsurface structures here, in the boundary portion of the mud volcano, is questionable. To overcome this problem, the new method was used to obtain a stacked section with all the possible diffraction energies. Subsequently, the stacked section underwent post stack depth migration. The final depth image proves the advantage of the new stacking operator for imaging in complex structures. Finally it could be concluded that this method could be used for imaging structures with sharp reflector truncations such as faults, diapirs, and unconformities.

**Keywords:** *conflicting dips, common reflection surface, common diffraction surface, complex media, seismic imaging, South Caspian Sea Basin*

---

## INTRODUCTION

Exploration geophysicists continue searching for fast and accurate seismic imaging algorithms that can be used for migrating large 3D survey data collected in geologically complex regions [Berkovitch et al., 2008; Pruessmann, 2008]. The objective of seismic imaging is to provide an image of the subsurface from multicoverage seismic reflection data by enhancing genuine reflection signals and suppressing unwanted energy in the form of coherent and random noise. However, recent advances in time and depth imaging and velocity model building resulted in the introduction of novel methods for imaging in complex structures. Some of those methods are path integral seismic imaging [Landa and Fomel, 2006], full waveform inversion [Robein, 2010], multifocusing method [Gelchinsky et al., 1999], hybrid linear and non-linear full waveform inversion [AlTheyab and Wang, 2013], polystack method [de Bazelaire, 1988], common reflection surface [Müller et al., 1999], reverse time migration [Baysal et al., 1983] and the Gaussian beam migration [Hill, 1990]. The common reflection surface (CRS) stack method and the common reflection surface-beam prestack depth migration [Garabito et al., 2012a], could partly resolve some of ambiguities in geological interpretation of seismic sections. However, some of these new methods belong to prestack migration methods beyond Kirchhoff (wave-equation and beam migrations), and some are referred to imaging by regularized iterative inversion [Biondi, 2006].

However, the main challenge for seismic imaging in structurally complex media is associated with the complexity of the wave-propagation phenomena. Important instances of these situations are intruded mud volcanoes or salt diapirs in sedimentary basins and the fault-folded structure; that in the viewpoint of geophysical prospecting, they make hydrocarbon-bearing structures.

Complex bodies such as salt diapirs or mud volcanoes are illuminated by many wave paths that cannot be considered by conventional one-way wave equation techniques. In such areas, the combination of the model building and the migration is the key to a successful imaging [Robein, 2010]. However, some of those methods need the velocity model as accurate as possible, while the common reflection surface proved that regardless of the velocity model accuracy, result of the post-stack time migration could be comparable to the result of the pre-stack depth migration.

Furthermore, in contrast to certain conventional seismic imaging methods like the common midpoint stack, the common reflection surface stack makes use of the full multicoverage data volume during the imaging process. The common reflection surface method uses a stacking operator that describes the reflection moveout response for inhomogeneous media. In contrast to the common mid-point, the common reflection surface method does not directly depend on the macro stacking velocity model.

## FROM CRS TO CRS-BEAM-PSDM

In classical normal move-out correction and common mid-point stack method, the stacked section is obtained by summation over a curve along the offset coordinate (green curve Fig. 1b). The concepts of using second order traveltimes approximations for stacking can be generalized to include also the midpoint coordinate. The stacking operator in 2D is then no longer a trajectory in time/half-offset/midpoint coordinates, but is a stacking surface, which extends not only in the offset, but also in the midpoint direction (Fig. 1a).

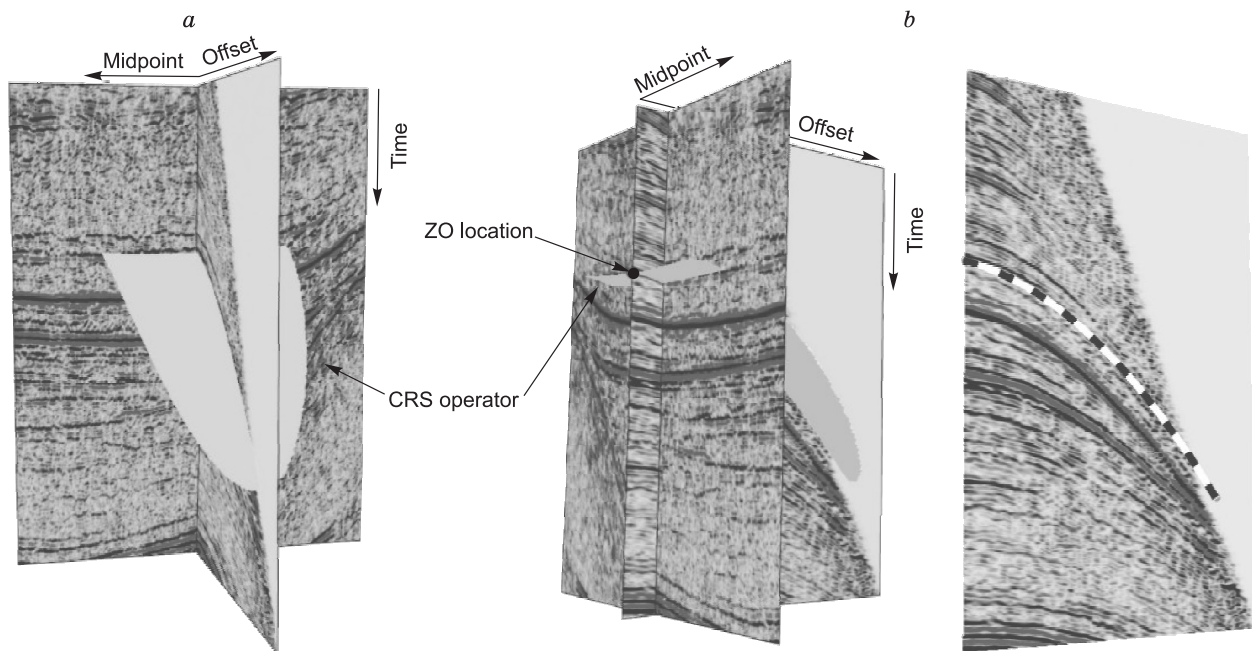


**Fig. 1. Different stacking operators. (a), the CRS stack operator in time, midpoint and half-offset domain highlighted in green and (b) the NMO summation trend shown by green line [13].**

Jäger [1999] showed that the parameters of that surface could be approximated for limited offsets and limited midpoint apertures by a parameterized function of distance to the normal ray emergence point and half-offset by:

$$t_{\text{hyp}}^2(x_m, h) = \left[ t_0 + \frac{2\sin\alpha(x_m - x_0)}{v_0} \right]^2 + \frac{2t_0\cos^2\alpha}{v_0} \left[ \frac{(x_m - x_0)^2}{R_N} + \frac{h^2}{R_{\text{NIP}}} \right] \quad (1)$$

where,  $\alpha$  is the emergence angle of the normal ray at  $x_0$ ,  $R_N$  is the radius of the wave front curvature of a hypothetical normal wave,  $R_{\text{NIP}}$  is the radius of wave front curvature of hypothetical normal-incidence-point (NIP) wave and  $h$  is the offset. Figure 2a shows the shape of the common reflection surface operator in time, midpoint and half-offset domain obtained by Equation (1). Compared to conventional stacking methods, the number of traces contributing for stacking in each zero offset sample is considerably increased in the common reflection surface stack method. So, it results in an improvement of signal to noise ratio [Heolmann et al., 2004; Mann et al., 2007; Menyoli et al., 2004]. Zhang et al. [2001] introduced the common offset common reflection surface stack method. The common offset common reflection surface stacking operator is macro-model independent and fully automatically determined by means of a coherency analysis. In contrast to conventional stacking methods, the common offset common reflection surface stack uses the full multicoverage data volume in the stacking procedure as it is not restricted to specific gathers (Fig. 2b). Bergler [2001] showed that the common offset common reflection surface stacking technique gives noteworthy results with respect to the stacked common offset section. However, this method could not solve the problem of conflicting dips. Höcht [2006] mentioned that conflicting dips often pose a problem when using a single operator. Later on, Höcht et al. [2009] introduced an interpolation scheme that was called operator oriented common reflection surface interpolation.

In this method, one operator may contribute to the construction of several target samples. Vice versa, a target sample might receive contributions from different operators. The use of multiple operators for a single target sample stabilizes the interpolation results and implicitly allows several contributions in case of interfering events. However, Soleimani [2009] mentioned that due to the considerable computational expense, common-reflection-surface interpolation is limited to work in subsets of the prestack data. Baykulov [2009] introduced the partial common reflection surface stack method which calculates a stacking surface around a specified point defined by its offset and travel time coordinates in a chosen common mid-point location and performs summation of data along that surface.

The partial common reflection surface stack is shown in Fig. 3a. This surface coincides locally with the conventional common reflection surface, but the size of the partial common offset common reflection surface is smaller. However, Baykulov [2009] mentioned that the partial common reflection surface stack method needs

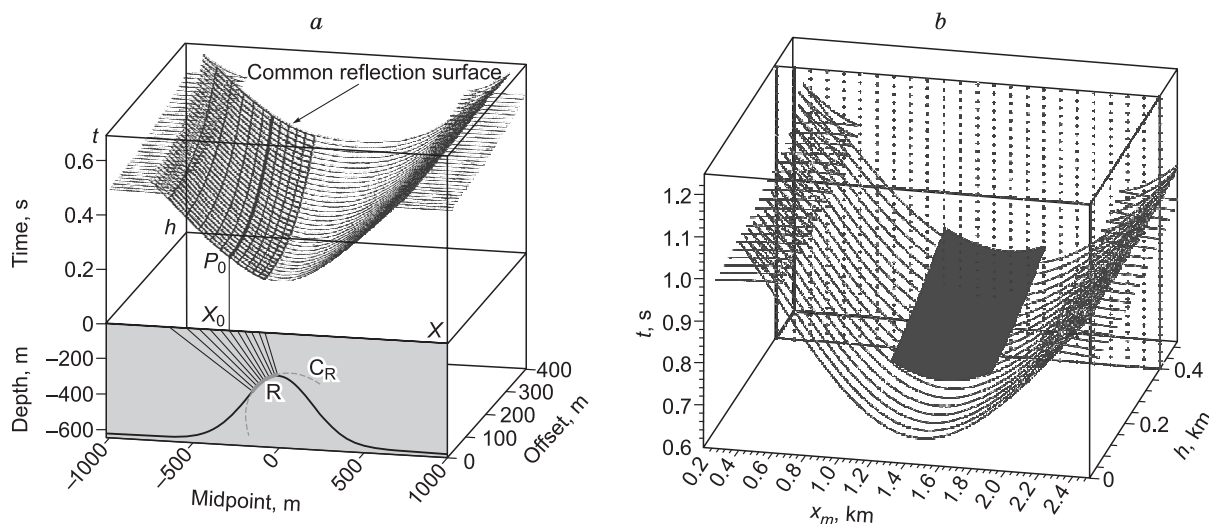


**Fig. 2. (a) Lower panel (front): 2-D medium with two homogeneous layers about a half-space separated by curved and smooth interfaces. Common Offset travel time curves (blue color) related to primary reflections of the second interface with the CRS travel time approximation (red color) associated with point  $P_0$ . (b) the Common Offset CRS surface. (Figure (a) from [Zhang et al., 2001] and (b) from [Bergler, 2001]).**

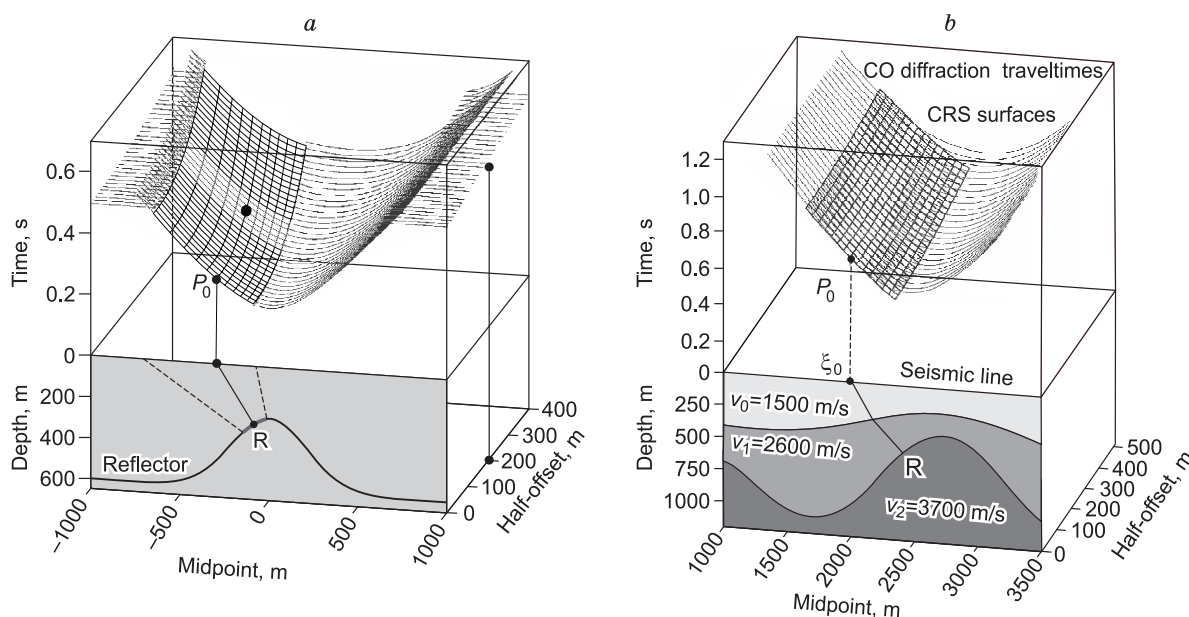


**Fig. 3. (a) The partial CRS stack performs the summation of data around the specified point on a CMP travel time curve (magenta line) and assigns the result to the same point in a newly generated CRS super gather. (b) The red lines are the CRS stack travel times related to the point  $P_0$  in the ZO plane. The blue lines are the Common-Offset diffraction travel times to define the stacking surface for the point R on the second reflector. (Figure (a) from [Baykulov, 2009] and figure (b) from [Garabito et al., 2012b]).**

further investigations on the conflicting dips problem. Yang et al. [2012] called the phenomenon caused by conflicting dips problem as ‘dip discrimination phenomenon’. Their common reflection surface stack with the output imaging scheme is a novel technique to implement a common reflection surface stack based on a unified Kirchhoff imaging approach.

In the latest investigation on the common reflection surface method, Garabito et al. [2012b] developed a new procedure of prestack depth migration based on the Kirchhoff migration integral and the beam stack using the common reflection surface stacking operator (Fig. 3b).

## INTRODUCTION TO THE CONCEPT OF CDS OPERATOR

One of the most serious problems in the common reflection surface method is solving the problem of conflicting dips. None of those methods emphasizes diffraction events; therefore they would have problems to image abrupt truncation in reflectors, such as faulting, salt diapir or mud volcano body. Mann [2002] introduced the extended search strategy in the common reflection surface method. In the general search strategy of the common reflection surface stack method, only one angle is respected as the optimum emergence angle. Whereas in the extended search strategy for defining the emergence angle of the central ray and producing the stacking surface, only those angles in the angle range that were above the user predefined relative threshold were considered for coherency analysis. Garabito et al. [2011] used the separation of reflections from diffractions and introduced the formulation of diffraction stack surface. This surface is shown in Fig. 4a. In this method, only one stacking surface would be selected after coherency analysis for the selected sample. It also did not mention that if this operator could resolve the problem of conflicting dips or not. In the new operator that is going to be addressed here, the idea of dip moveout was used to overcome the problem of conflicting dips. In conventional imaging, the dip moveout operator provides the correct amount of lateral moveout for each dip. Since different parts of dip moveout operator correspond to different dips, the conflicting dip problem is also correctly resolved.

However, in the common reflection surface stack method, and other improvements on it, only one stacking surface, that is selected by coherency analysis, is used for imaging the considered sample. This surface is also related to the most dominant events in the section that passes through the sample. Therefore, in the case of the conflicting dips problem, the common reflection surface method will fail to consider more than one event for one sample. Here, the idea to use more than one stacking surface by considering all possible dips for each sample was used to overcome the problem of conflicting dips. This idea means that the operator treats with each sample like as a diffraction point. In this method, all possible common reflection surface operators are contributed into stacking for each zero offset sample. The entire emergence angles of the central ray within the search range with any coherence value will make a stacking surface by defining an angle increment,  $da$ . Thus in the  $(x_m, t, h)$  space, not only one stacking surface, but many surfaces that are equal to the number of the emergence angles in the angle range are produced. These operators are shown in Fig. 4b (only three of tens of operators are shown for simplicity and better clarity).

The number of conflicting dips is not concerned here, because any present dip will contribute into stacking for each sample. Resolving the problem of conflicting dips with this method will enhance the usually weak

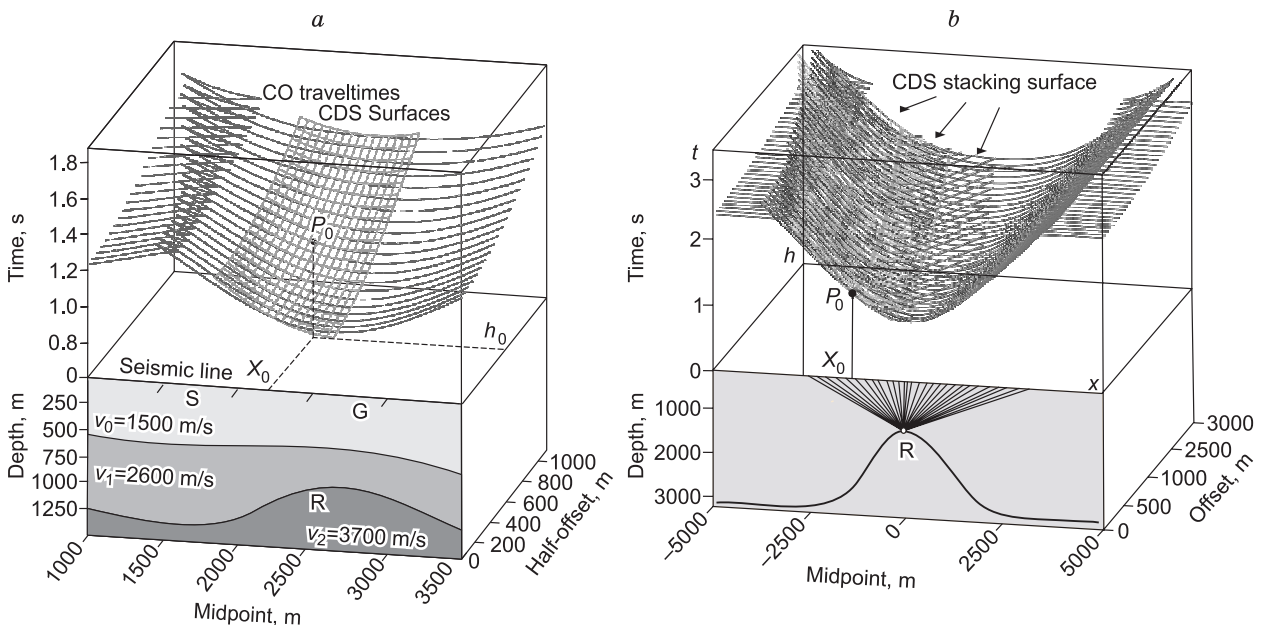


**Fig. 4. (a) Lower panel (front): 2-D medium with two homogeneous layers about a half-space separated by curved and smooth interfaces. A finite offset central ray is shown, where  $x_0$  is the midpoint and  $h_0$  is the half-offset. Upper panel: CO travel time curves (blue color) related to primary reflections of the second interface with the CDS operator (green color) associated with  $P_0$ . (b) The new introduced CDS operator volume stack. Against all the previous figures stated before, it contains all the possible surfaces that each one is related to an event with different dips in a sample (Figure (a) from [Garabito et al., 2011]).**

diffraction events in the stacked section. As the new strategy not only addresses reflection events but in particular diffraction events, it is called the common diffraction surface (CDS) stack method. Here the number of contributing events also equals to the number of stack surfaces, thus all of the operators contribute into stacking. None of these operators are a higher priority than the others; all are in a same level of importance. For a fixed emergence angle  $\alpha$  in equation 1, the only attribute to be searched for is a combination of  $R_{NIP}$  and  $R_N$ . In a theoretical point of view, the new curvature could be any combination of  $R_{NIP}$  and  $R_N$ . However, as it was mentioned by Mann [2002], for diffraction point,  $R_{NIP} = R_N$ . Thus, the combination of these curvatures here is called  $R_{CDS}$ . So the equation of the CRS will reduce to the following:

$$t^2(x_m, h) = \left( t_0 + \frac{2 \sin \pm}{v_0} (x_m - x_0) \right)^2 + \frac{2 t_0 \cos^2 \pm}{v_0 R_{CDS}} \left( (x_m - x_0)^2 + h^2 \right) \quad (2)$$

That is called the common diffraction surface stacking operator. To make the common diffraction surface operator for a zero offset sample, the number of operators should be defined according to a predefined angle range and angle increment that would be defined according to the complexity of the structure. Widening the angle search range and shortening the angle increment step leads to increasing computation time to search for  $R_{CDS}$ .

The strategy used here differs from the simplified search of Garabito et al. [2012], the extended search strategy of Mann [2002], and the pragmatic search strategy of Müller [1998]. In this strategy, the only remaining attribute to be searched for is the  $R_{CDS}$  attribute. The first thing that should be defined by the user is the range of considered emergence angles along with a suitable angle increment. The larger the search range, the more computational time. The target zone, the aperture and the range for minimum and maximum stacking velocities are defined for the normal common reflection surface search strategy. For a range of values of  $R_{CDS}$  to be tested, the shape of the operator could be defined in terms of a moveout range. By coherency analysis, the optimum value of  $R_{CDS}$  can be calculated in the next step. Although this initial maximum could be further refined, this would be computationally very expensive and would have little impact on the final stack result. Now, by knowing the optimum value of  $R_{CDS}$  and the emergence angle  $\alpha$ , equation (2) defines the shape of the stacking operator for the specified sample. According to the user given angle increment  $d\alpha$ , the same procedure for the same sample is performed for the next defined angle ( $\alpha + d\alpha$ ) within the angle range and the next operator for the same sample will be shaped. The angle increment always has to use a sufficiently fine angle grid, even if there is only one contributing event. Otherwise, it might simply miss the contributing dips. This procedure is repeated over the entire angle range and all common diffraction surface samples. At the final step, all events are able to simulate their interferences by superposition. Figure 5 shows the simplified flowchart of the proposed strategy for the common diffraction surface stack method.

Enhancing diffractions in the common diffraction surface stacked section will further image the geological structures that are responsible for making those diffractions, like as faults, salt diapir or mud volcano body and other similar structures. In this study, we used a 2D line for seismic imaging the mud volcanoes in the South Caspian Sea Basin, the Gorgan Plain, in North East of Iran with the introduced common diffraction surface stack method.

## MUD VOLCANOES IN THE SOUTH CASPIAN BASIN AND STUDY AREA

In complex media, mud volcanoes as a natural phenomenon have attracted geoscientists for a long time. They have many similarities in appearance to that of magmatic volcanism but widely differ in origin. Many authors describe mud volcanoes as simple topographical features complicating the surface morphology [Jakubov et al., 1971], without taking into account that these landforms are expression of a remarkable natural process initiated deep in the sedimentary succession. Mud volcanoes are geological structures formed as a result of the emission of argillaceous material on the Earth's surface or the sea floor. The term mud volcano system is coined to describe the set of structures associated with the constructional edifice and feeds complex that connects the mud volcano to its stratigraphic source [Basu et al., 2012]. The majority reported mud volcanoes occur at active plate margins which lead many authors to suggest that tectonic stress, mainly compressional, is the main driving mechanism for mud volcanoes. The largest and best cone-shaped mud volcanoes as well as the most active ter-

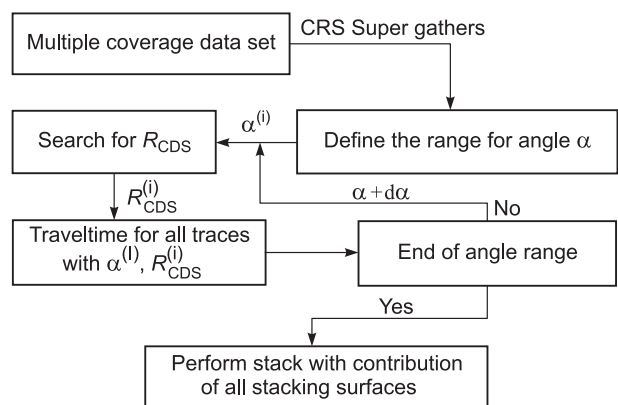


**Fig. 5. Simplified flowchart of the improved strategy.**

restrial mud volcano area with the greatest number of mud volcanoes in the world occur at a belt centered in the Baku region of the Caspian Coast, Eastern Azerbaijan. This belt starts from the Mediterranean Ridge and adjacent land areas in Sicily, Albania and Southern, Central and Northern Italy. Continuing past the forelands of Eastern Carpathians in Romania, Kerch and Taman Peninsula through the Black Sea, the belt turns to the south in the area of Southern Caspian Sea and Gorgan Plain in Iran, passing the Makran coast of Pakistan and Southern Himalayas, ending in Burma [Dimitrov, 2002]. Figure 6a shows geological blocks and distribution of mud volcano in the South Caspian Sea basin as a part of this belt. The South Caspian Sea basin is one of the most important mud volcano bearing basins with varying size of mud volcanoes from small to giant (in some reports;

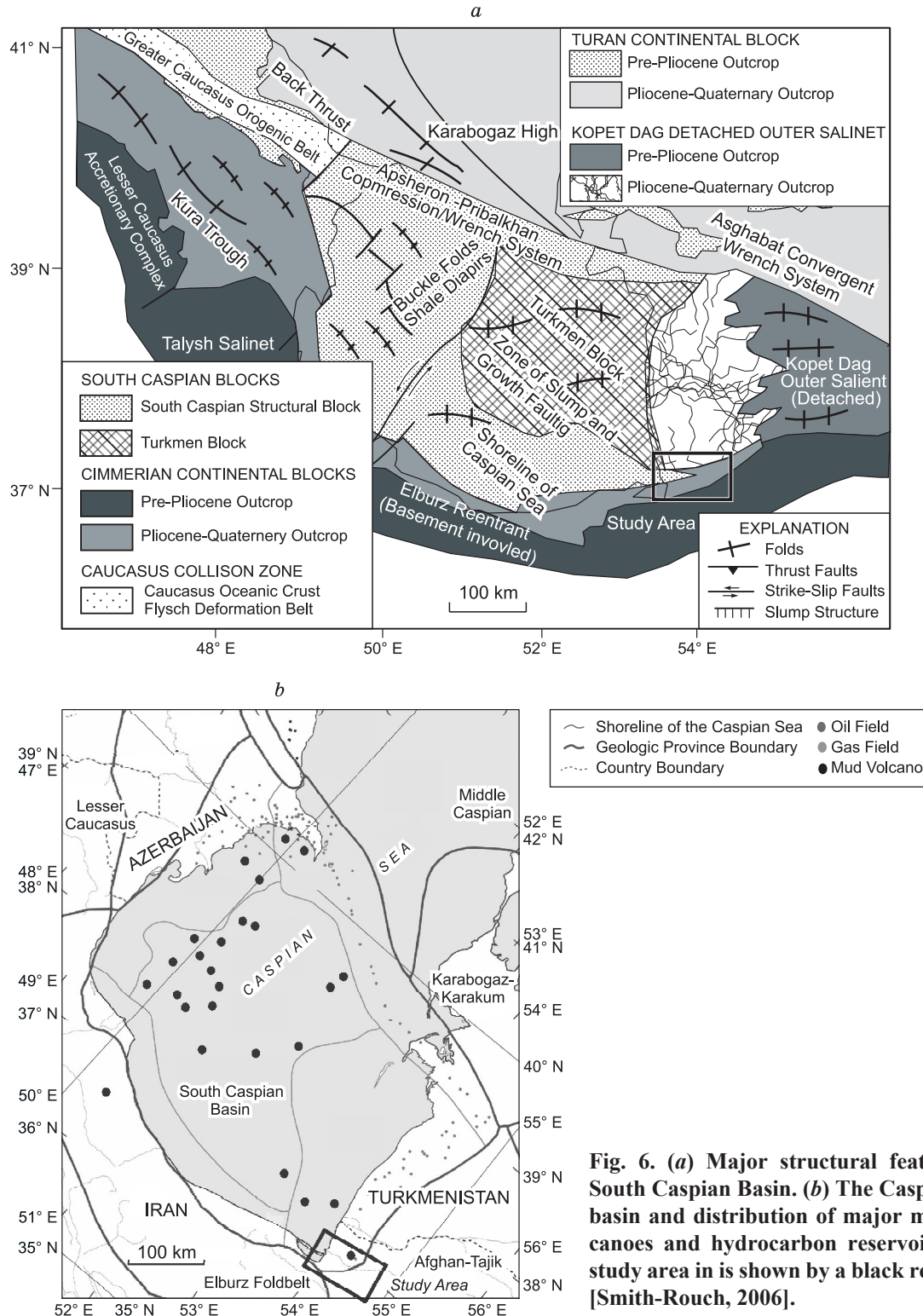


**Fig. 6. (a) Major structural features in South Caspian Basin. (b) The Caspian Sea basin and distribution of major mud volcanoes and hydrocarbon reservoirs. The study area in is shown by a black rectangle [Smith-Rouch, 2006].**

10 km wide and 1.4 km thick, overlying an oval caldera 1.2–1.6 km in width and 0.5 km in depth) [Davies and Stewart, 2005]. Most of the mud volcanoes in the South Caspian Sea Basin consist of an extruded submarine mud bi-cone. A 3D seismic study on the mentioned giant mud volcano in the South Caspian Sea Basin showed that their caldera narrows downwards into a zone of collapsed country rock forming a downward tapering cone [Davies and Stewart, 2005]. In the other seismic modeling of the South Caspian Sea Basin, it was stated that wall rock erosion and compaction of the intruded zone leads to the collapse of a downward-tapering cone enveloping the cylindrical zone, capped by ring faults [Davies and Stewart, 2006]. Mud volcanoes get buried during basin subsidence and can look like intrusive laccoliths at first glance on seismic data. Reactivation of mud flow through a conduit system generates a stack of superimposed mud volcanoes through time. Large volcanoes continue to dewater during burial and may locally remobilize [Davies and Stewart, 2006]. In another study, a 3D/4C and 4D Ocean Bottom Cable (OBC) program was used to seismically image mud volcanoes in the South Caspian Sea in the Azerbaijan offshore [Bouska, 2007].

The study area is located in the shoreline of the Caspian Sea and the Kopet Dag zone, shown by rectangle in Fig. 6b. The Kopet Dag region trends for 700 km south of the Caspian Sea, and passes northeast of Iran and southwest of Turkmenistan (Fig. 6a). It separates the Turkmen Block from central Iran. The height of the region ranges up to 3000 m in some parts, which is 2000 m higher than the Turkmen foreland basin to the north. Jurassic–Miocene marine carbonates and clastics were deposited across the region are now deformed into a series of folds and thrusts. These are broadly convex northwards, and curve into the trend of the range parallel to the right-lateral Ashgabat fault at the northern margin of the region (Fig. 6a). Focal mechanisms in this area show north-to-south overthrusting on gently north-dipping planes [Smith-Rouch, 2006]. The Gorgan region is a part of the Kopet Dag zone located in northeast Iran in two different geological zones. These two zones are among the several sedimentation basins that are distributed between Iran and Turkmenistan. The region is made of thick sediments from Jurassic to Miocene age [Weinelt and Brückmann, 2011].

These sediments are made of shale, limestone, marl, sandstone, and sometimes conglomerates and evaporates. This sequence is beneath an unconformity of Palaeocene conglomerates. This region is famous for its mud volcanoes as most are related to gas reservoirs (Fig. 6b). Figure 7 shows the exact seismic line in the study area. This seismic line was designed based on the previous gravimetry acquisition. Figure 7 shows the gravity map of the study area that defines possible locations of mud volcanoes (and related hydrocarbon reservoirs) with low gravity value. Thus the seismic line that was selected for this study had been designed in order to pass through most of the structural events (Black line in Fig. 7).

The aim of seismic experiment in this region was defining favorable structure for hydrocarbon reservoirs. So a 2D seismic project was designed in the area and the largest line with more complex structures was selected here for seismic imaging. Length of the seismic line is about 48 km with 680 shot points and maximum offset of 3458 m. The seismic data contain approximately 1900 common midpoint records (some of them from end of the line were removed due to dramatically low fold) with spacing near 25 m. The maximum fold of the line was 35, which make it a low fold data. A brief introduction of the seismic line is shown in table 1. It should be noted that in a 2D seismic survey, the implicit assumption is that the earth is a cylinder, with the axis orthogonal to the survey. If this underlying assumption is fulfilled, the image obtained by 2D seismic interpretation is an accurate representation of a vertical section of the subsurface. However, when this assumption is not fulfilled, 2D seismic imaging produces a distorted image of the subsurface. The most severe problem in 2D seismic imaging is out of plane reflection. Geological structures are 3D in real world, so it is usual that diffractor points that lay out of the plane of acquisition, introduce additional reflection to the data. These reflections are incorrectly back propagated in the earth along the vertical plane passing through the acquisition direction and imaged in wrong position [Biondi, 2006]. To image the diffractor at its correct location, 3D imaging

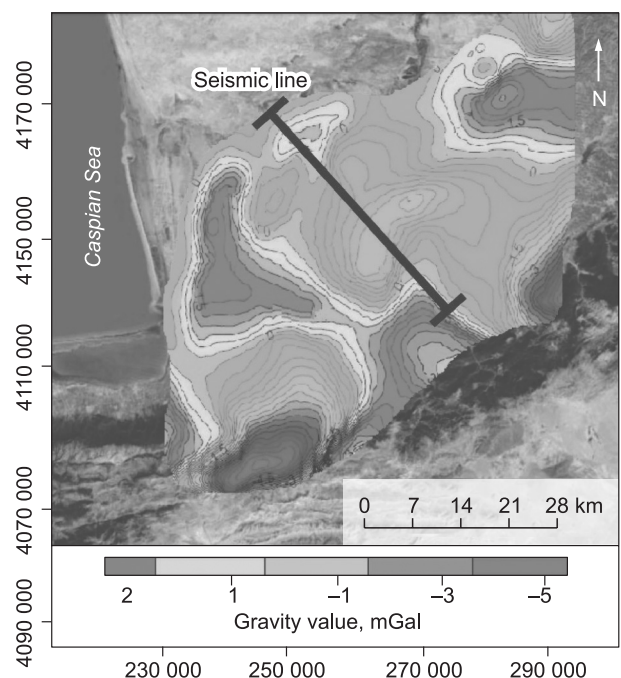


**Fig. 7.** Gravity map of the study area that was the base of seismic acquisition design. The seismic line is shown by black line (gravity map from [Baghzendani et al., 2015]).

Table 1. **Geometry of the seismic line used in this study**

Mid-point and offset geometry		Shot and receiver geometry	
CMP numbers	1900	Number of shots	680
Maximum fold	35	Shot spacing	70 m
CMP spacing	25 m	Number of receiver	99
		Receiver spacing	50 m
Frequency content		Recording parameters	
Frequency range	8 – 100 Hz	Total recording time	7 s
Dominant frequency	20 Hz	Sampling interval	4 ms

is necessary to be applied for back-propagating the recorded reflection along an oblique plane. However, in this study, there was no 3D seismic data available. Based on the gravity map of the study area (Fig. 7), it was assumed that the 2D seismic line is orthogonal to the general trend of the region and passes over top of the mud volcano in the subsurface. Thus, care should be taken in interpretation of the final depth image.

### IMAGING BY THE CRS AND THE CDS STACK METHODS

The common reflection surface stack method was used by several researchers for depth model building in simple or complex structures [Landa et al., 1999]. The seismic data of the Gorgan region has been processed with the optimized common reflection surface stack to obtain the optimized stacked section shown in Fig. 8. There exists an unconformity in the section that separates the overlaying quaternary sediments from the underlying sediments which consist of a sequence of shale, limestone, marl, and sandstone. The upper sediments are gently dipping to the right of the section. The underlying layers are dipping to the left in some parts and to the right in the other parts. Some faults are imaged in the upper layers in the right part of the section. Detecting and tracing the faults is difficult in this section. This difficulty is due to the smoothing nature of the common reflection surface stack method that removes the sharpness of events on the section. It also relates to the type of the rocks of the layers that are made of alluvium, river, and deltaic sediments that can be easily deformed by the stresses and creates no sharp edges. However, these faults will be better imaged in a migrated section or by applying some other imaging methods like the common diffraction surface stack. The big concern in this section is to image the mud volcano boundaries below the unconformity. The study area has two mud volcanoes in the left and one in the right. The two minor mud volcanoes are somehow captured by the seismic line and are located in the left part of the section. However, some diffraction events that are due to the contacts of the mud volcano boundary with the dipping layers are clear. The effect of the major mud volcano can also be seen in the lower right part of the section.

In most cases, applying partial stack migration or pre-stack depth migration in severely complex media gives an acceptable image of the subsurface, but in some cases, imaging beneath the complex structures is a challenging task. In an attempt to image the semi-complex structure of the Gorgan region, acceptable results could not be drawn by conventional and common reflection surface stack methods, due to strong lateral velocity changes below the unconformity. In most part of the section shown in Fig. 8, the events were cleared and more structures could be observed. However, the problem of detecting the boundary of mud volcanoes in the

left part still remains. Most of the problems of conflicting dips in the section happen in events between dipping layers below the unconformity and horizontal layers above the unconformity. To resolve this problem the common diffraction surface stack method was applied on the data (Fig. 9). As can be seen at the first glance, the quality of the stacked section and the signal-to-noise ratio is better in the common reflection surface stack method. It should be noted that the common diffraction surface operator images

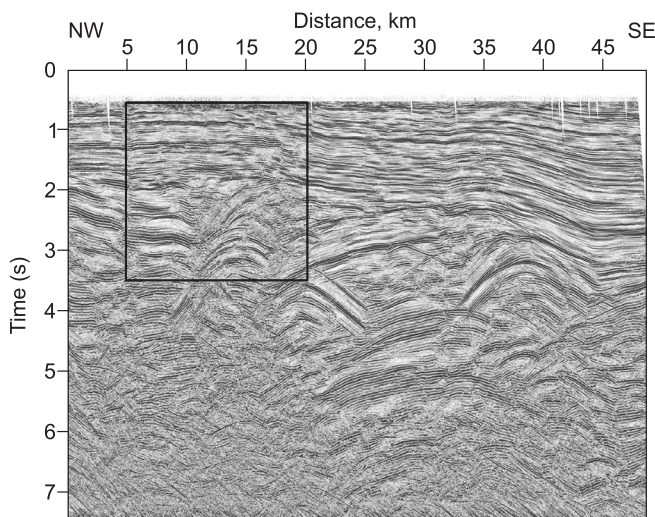
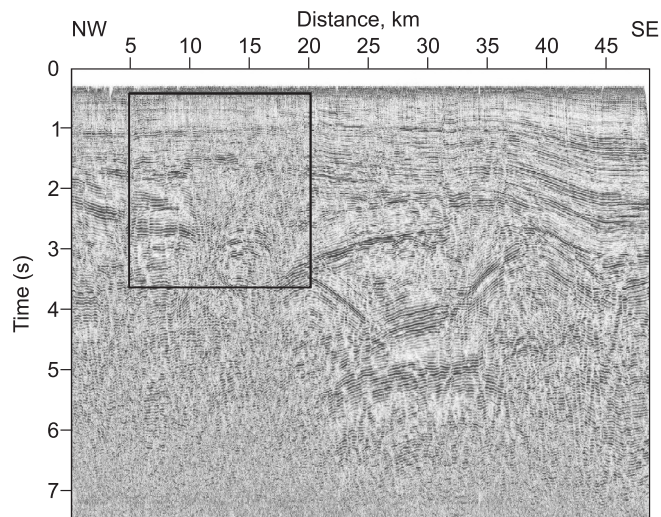


**Fig. 8. The CRS stack section. The unconformity and diffraction patterns due to the mud volcanoes are clearly seen on the section. Black rectangle shows part of the section showing in subsection in Fig. 10a.**

**Fig. 9. The CDS-stacked section. Black rectangle shows part of the section showing in subsection in Fig. 10b.**



all the events exist in the events in the prestack data. Thus, the common diffraction surface stacked section might not be comparable with the common reflection surface result in case of signal to noise ratio. However, truncations of events are better shown in the common diffraction surface result and more diffractions are also imaged. Therefore it is supposed that the common diffraction surface stacked section will have better performance in migration procedure. This will make the imaging methods applicable to locate the exact location of faults and show their trends. The problem of conflicting dips is also solved by the common diffraction surface method.

Differences are shown with more detail in a subsection in Fig. 10. Result of the common reflection surface imaging (Fig. 10a), shows better continuity of events, while the intersections of events in deeper parts are not well resolved. Figure 10b shows the same part in the common diffraction surface stacked section. The quality of the section in Fig. 10a is improved, but more details of events are shown better in the common diffraction surface stacked section. Resolving the problem of conflicting dips and better imaging of faults and dipping events is the main advantage of the common diffraction surface imaging, shown in Fig. 10b. However, it is expected to image more details in a migrated section obtained from the common diffraction surface result rather than migration of the common reflection surface.

It should be mentioned that since the common diffraction surface stack operator consider a stacking surface for all emergence ray angles, it might increase the background noise in the stacked section. Nevertheless, it is nothing to be concerned about, because most of the relevant events will provide usable energies for migration operator in the next steps.

Thus, it could be concluded that although the signal to noise ratio is lower in the common diffraction surface stack result, it would be a better input for migration procedure that will image more details of the section. Therefore, selection of the common reflection surface or the common diffraction surface method is a trade-off between noise and details. In simple layered media, the common reflection surface method will preserve better continuity of the reflectors while failing to show more details in complex structure. However, the common diffraction surface stack method might increase the background noise in the stacked section, but it will compensate that with a dramatic increase in imaging more detail in complex structures in post stack depth migration. This is obvious in comparing the final migrated images of both methods.

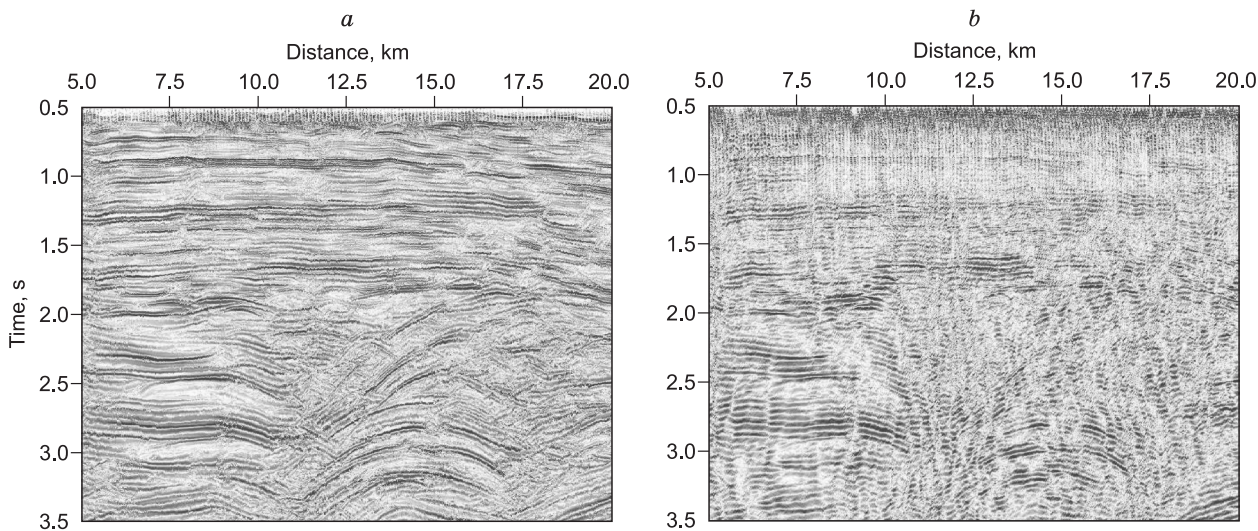


**Fig. 10. Subsection of the CRS-stacked section (a) and corresponding subsection of the CDS-stacked section (b) of the Gorgan region data.**

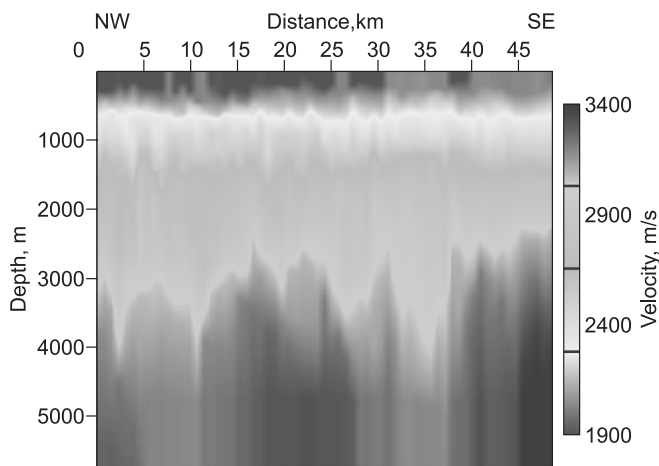


**Fig. 11. The velocity model used for migration. The low velocity zones are due to mud volcano or might be the reason of gas chimney.**

### INTEGRATION PROCEDURE FOR VELOCITY ANALYSIS AND MIGRATION

To perform migration on the stacked sections, a sufficiently accurate velocity model of the region was needed. The velocity model was obtained by integration procedure for migration velocity analysis [Alaei, 2006]. The procedure has four main stages: initial model generation, regional velocity update, detailed high-resolution velocity update and final model generation. It is based on the depth tomography of migrated gathers. Constraining the pre-stack depth migration velocity analysis by appropriate a priori information is an important part of the velocity analysis process [Duvencck, 2001]. The area has several complexities including faulted blocks, different style of deformation at subsurface and strong lateral velocity variation. A variety of a priori information has been used at four velocity estimation steps to constrain the migration velocity analysis procedure. Some rock units in the studied area show a depth-independent velocity behavior. So when the configuration of main structural elements is mapped, the interval velocity of such units is updated with controlled horizon-based tomography. The final velocity model obtained with this strategy is fully consistent with the structural pattern of the area and also with the properties of individual rock units. The final velocity model is shown in Fig. 11.

The common reflection surface stacked and the common diffraction surface stacked sections were used as inputs for post-stack depth migration.

It should be mentioned that although the total recording time was 7 s, there is no usable information in times greater than 6 s. Therefore, only 6s of the data was used for migration procedure. The result of the migration performed on the common reflection surface stacked section is shown in Fig. 12. At the first glance, some of the geometrical distortions that were corrected by the migrated section are obvious in the section. The intersections of the dipping layers below the unconformity and the overlaying layers are better imaged. The faults in the upper right are also imaged well.

The result of migration performed on the common diffraction surface stacked section is shown in Fig. 13. The boundary of the mud volcanoes in the left part of the section that was of more concern than the other parts is imaged better here. The reflectors and other structures that caused the diffraction events in the stacked section can be seen clearly.

The common diffraction surface stack migrated section could better map the faults. Figure 14 shows two subsections of common reflection surface and common diffraction surface stack migrated section in detail. As it could be seen, mi-

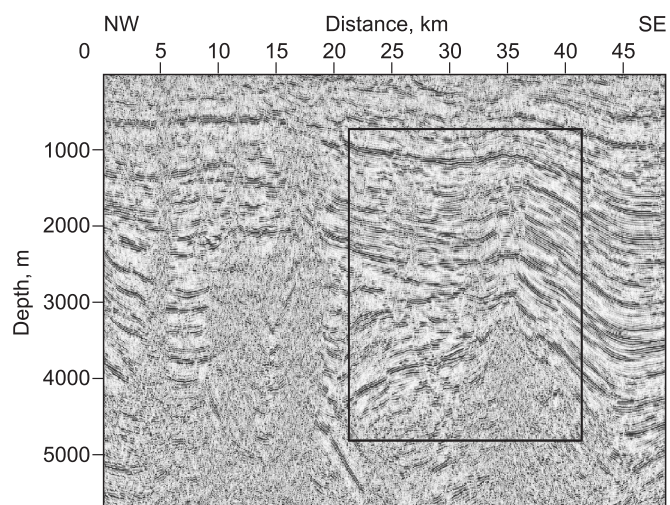


**Fig. 12. Defining the mud volcano boundary, layers, and faults on the CRS stack migrated section. Black rectangle shows part of the section showing in subsection in Fig. 14a.**

**Fig. 13. Defining the mud volcano boundary, layers, and faults on the CDS stack migrated section. Black rectangle shows part of the section showing in subsection in Fig. 14b.**

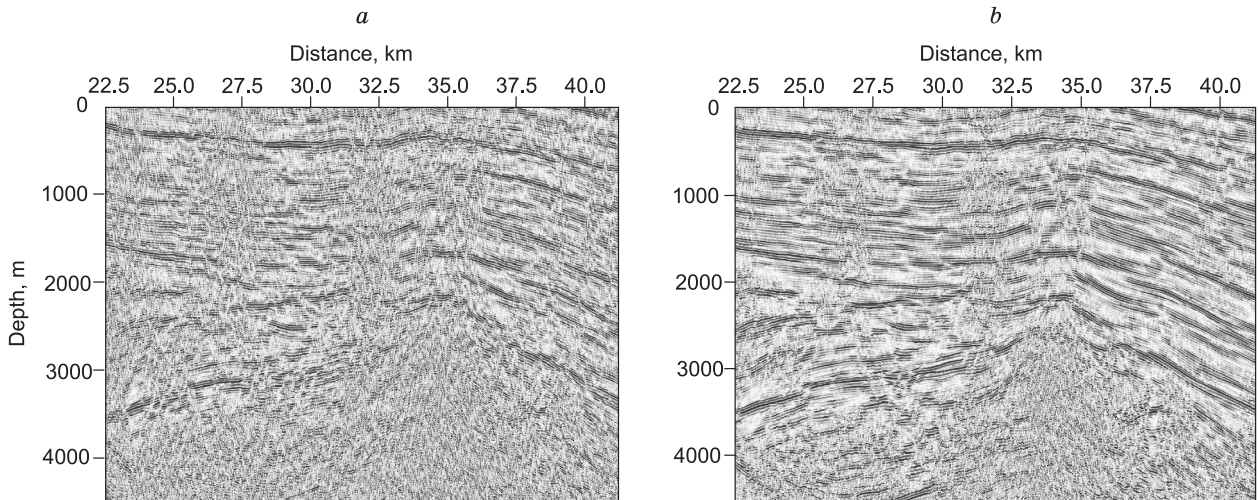
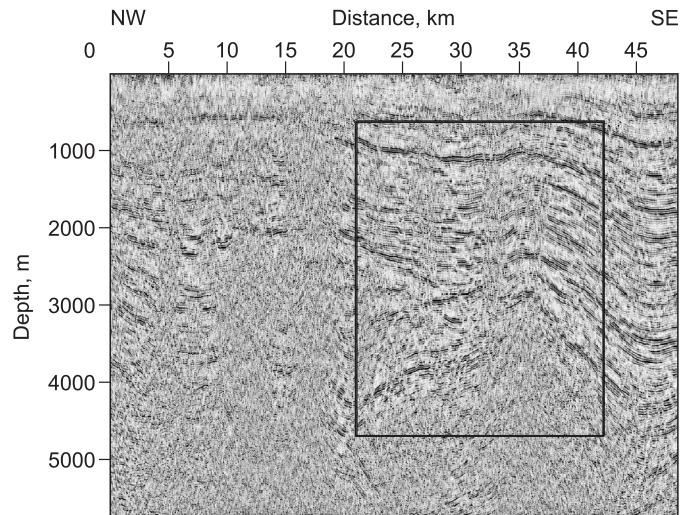


**Fig. 14. Subsection of depth migration on (a) the CRS stacked section and (b) on the CDS stack result. Migration on the CDS stack result shows well imaging of faults, mud volcano body, and wedge shape.**

gration on the common diffraction surface stacked section could better resolve the problem of conflicting dips and thus provide better imaging of faults and such geological events, like as mud volcano boundary. Finally the primary interpreted section is drawn in Fig. 15.

### CONCLUSIONS

The problem of imaging in complex structures such as folded areas, salt diapirs, or mud volcanoes, and the quality of the seismic sections in such situations cannot be properly solved by conventional stacking methods. The conventional processing steps have some limitations on imaging of such complex structures. The common diffraction surface stacked section followed by depth migration showed that it can be a method for imaging in complex structures. This mainly relates to the common diffraction surface stacking operator that gathers all the energies in data that might get lost in the other imaging methods. After conventional stacking, the data set was processed by the common reflection surface and the common diffraction surface stack methods. The velocity model was built by a new introduced migration velocity analysis technique and then used for post-stack depth migration. The migrated sections showed that they can clearly define the boundary of mud volcanoes that were not imaged well by other methods.

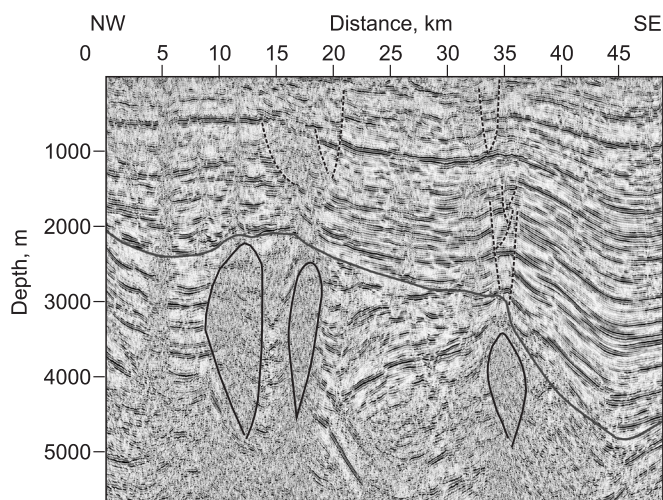


**Fig. 15.** The primary geological interpretation performed on the CDS stacked migrated section. Mud volcanoes, unconformity, and faults are shown on the section.

The near surface faults and the larger fault that continued to larger depths were also imaged better in the migrated section of the common diffraction surface stacked result. Therefore, it could

be said that the common diffraction surface stacked section provides suitable input for migration in regions with complex structure. The accuracy of the velocity model here is also not so much in concern.

#### REFERENCES

- Alaei B.** An integrated procedure for migration velocity analysis in complex structures of thrust belts // *J. Appl. Geophys.*, 2006, v.59, p. 89–105.
- AlTheyab A., X. Wang X.** Hybrid linear and non-linear full-waveform inversion of Gulf of Mexico data // SEG Annual Mtg. Houston, USA, 2013, p. 1003–1007.
- Baghzendani H.R., Aghajani H., Soleimani M.** Subsurface modeling of mud volcanoes, using density model and analysis of seismic velocity // *J. Mining Environ.*, 2015, v. 6, p. 31–39.
- Basu P., Verma R., Paul R., Viswanath K.** Mud volcanoes in deep water of Andaman Forearc Basin // *Geohorizons Symposium*, 2012, p. 26–31.
- Baykulov M.** Seismic imaging in complex media with the common reflection surface stack. Ph.D. Thesis, Hamburg University, 2009.
- Baysal E., Kosloff D.D., Sherwood J.W.C.** Reverse time migration // *Geophysics*, 1983, v. 48, p. 1514–1524.
- Bergler S.** The common-reflection-surface stack for common offset — theory and application. Master's Thesis, Universitat Karlsruhe, 2001.
- Berkovitch A., Belfer I., Landa E.** Multifocusing as a method of improving subsurface imaging // *The Lead. Ed.*, 2008, v. 27, p. 250–256.
- Biondi B.** 3D seismic imaging. SEG investigations in geophysics Series No. 14, Tulsa, Society of Exploration Geophysicists, 2006, 240 p.
- Bouska J.** 3D/4C and 4D ocean-bottom seismic surveys in the Caspian Sea // *Offshore Technology Conference*, Texas, U.S.A., OTC-18671-MS, 2007.
- de Bazelaire E.** Normal moveout revisited — inhomogeneous media and curved interfaces // *Geophysics*, 1988, v. 53, p. 143–157.
- Davies R.J., Stewart S.A.** Emplacement of giant mud volcanoes in the South Caspian Basin: 3D seismic reflection imaging of their root zones // *J. Geol. Soc.*, 2005, v. 162, p. 1–4.
- Davies R.J., Stewart S.A.** Structure and emplacement of mud volcano systems in the South Caspian Basin // *AAPG Bulletin*, 2006, v. 90, p. 771–786.
- Dimitrov L.I.** Mud volcanoes — the most important pathway for degassing deeply buried sediments // *Earth Sci. Rev.* 2012, v. 59, p. 49–76.
- Duveneck E.** Velocity model estimation with data-derived wavefront attributes // *Geophysics*, 2004, v. 69, p. 265–274.
- Garabito G., Oliva P.C., Cruz J.C.R.** Numerical analysis of the finite-offset common-reflection-surface traveltimes approximations // *J. Appl. Geophys.*, 2011, v. 74, p. 89–99.
- Garabito G., Stoffa P.L., Lucena L.S., Cruz J.C.R.** Part II, CRS-beam PSDM: Kirchhoff-beam prestack depth migration using the 2D CRS stack operator // *J. Appl. Geophys.*, 2012a, v. 85, p. 102–110.

- Garabito G., Stoffa P.L., Lucena L.S., Cruz J.C.R.** Part I — CRS stack: Global optimization of the 2D CRS-attributes // *J. Appl. Geophys.*, 2012b, v. 85, p. 92–101.
- Gelchinsky B., Berkovitch A., Keydar S.** Multifocusing homeomorphic imaging Part 1. Basic concepts and formulas // *J. Appl. Geophys.*, 1999, v. 42, p. 229–242.
- Heilmann Z., Mann J., Duveneck E., Hertweck T.** CRS-stack-based seismic reflection imaging — a real data example. Extended Abstracts, 66th Conf. Eur. Assn. Geosci. Eng., 2004.
- Hill N.R.** Gaussian beam migration. *Geophysics*, 1990, v. 55, p. 1416–1428.
- Höcht G.** Parameter-oriented CRS imaging. SEG/New Orleans Annual Meeting Extended Abstracts, 2006.
- Höcht G., Ricarte P., Bergler S., Landa E.** Operator-oriented CRS interpolation // *Geophys. Prosp.*, 2009, v. 57, p. 957–979.
- Jakubov A.A., Ali-Zade A.A., Zeinalov M.M.** Mud volcanoes of the Azerbaijan SSR. Atlas. Baku, Azerbaijan Academy of Science, 1971.
- Jäger R.** The common reflection surface stack: theory and application. Diploma Thesis, University of Karlsruhe, 1999.
- Landa E., Gurevich B., Keydar S., Trachtman P.** Application of multifocusing method for subsurface imaging // *J. Appl. Geophys.*, 1999, v. 42, p. 283–300.
- Landa E., Fomel S., Moser T.J.** Path-integral seismic imaging // *Geophys. Prosp.*, 2006, v. 54, p. 491–503.
- Mann J.** Extensions and applications of the common-reflection-surface stack method. Berlin, Logos Verlag, 2002.
- Mann J., Schleicher J., Hertweck T.** CRS stacking; A simplified explanation. 69th EAGE Conference & Technical Exhibition, London, 2007.
- Menyoli E., Gajewski D., Huebscher C.** Imaging of complex basin structure with common reflection surface (CRS) stack method // *Geophys. J. Int.*, 2004, v. 157, p. 1206–1216.
- Müller T.** Common reflection surface stack versus NMO/stack and NMO/DMO/stack // Extended Abstracts, 60th Conf. Eur. Assn. Geosci. Eng., 1998, Session 1-20.
- Müller T.** The common reflection surface stack method—seismic imaging without explicit knowledge of the velocity model. Ph.D. Thesis, University of Karlsruhe, Germany, 1999.
- Pruessmann J., Frehers S., Ballesteros R., Caballero A., Clemente G.** CRS based depth model building and imaging of 3D seismic data from the Gulf of Mexico // *Geophysics*, 2008, v. 73, p. 303–311.
- Robein E.** Seismic imaging: A review of the techniques, their principles, merits and limitations. Eur. Assoc. Geosci. Eng. Publ., Netherlands, 2010, 244 p.
- Smith-Rouch L.S.** Oligocene–Miocene Maykop/Diatom total petroleum system of the South Caspian Basin province, Azerbaijan, Iran, and Turkmenistan. USGS report, Bulletin 2201–I, 2006.
- Soleimani M.** Common reflection surface (CRS) stack accounting for conflicting dip situation by considering all possible dips. Ph.D. Thesis, University of Shahrood, Iran, 2009.
- Weinelt M., Brückmann W.** Mud volcanoes in the South Caspian Basin: Activity inferred from ENVISAT ASAR images // GRSG/OGEO Workshop, 2011, p. 1–27.
- Yang K., Bao-shu C., Wang X.J., Yang X.J., Liu J.R.** Handling dip discrimination phenomenon in common reflection surface stack via combination of output imaging scheme and migration/demigration // *Geophys. Prosp.*, 2012, v. 60, p. 255–269.
- Zhang Y., Bergler S., Hubral P.** Common-reflection-surface (CRS) stack for common offset // *Geophys. Prosp.*, 2001, v. 49, p. 709–718.

*Рекомендована к печати 29 января 2016 г.  
В.С. Селезневым*

*Поступила в редакцию 10 февраля 2014 г.,  
после доработки — 17 сентября 2015 г.*